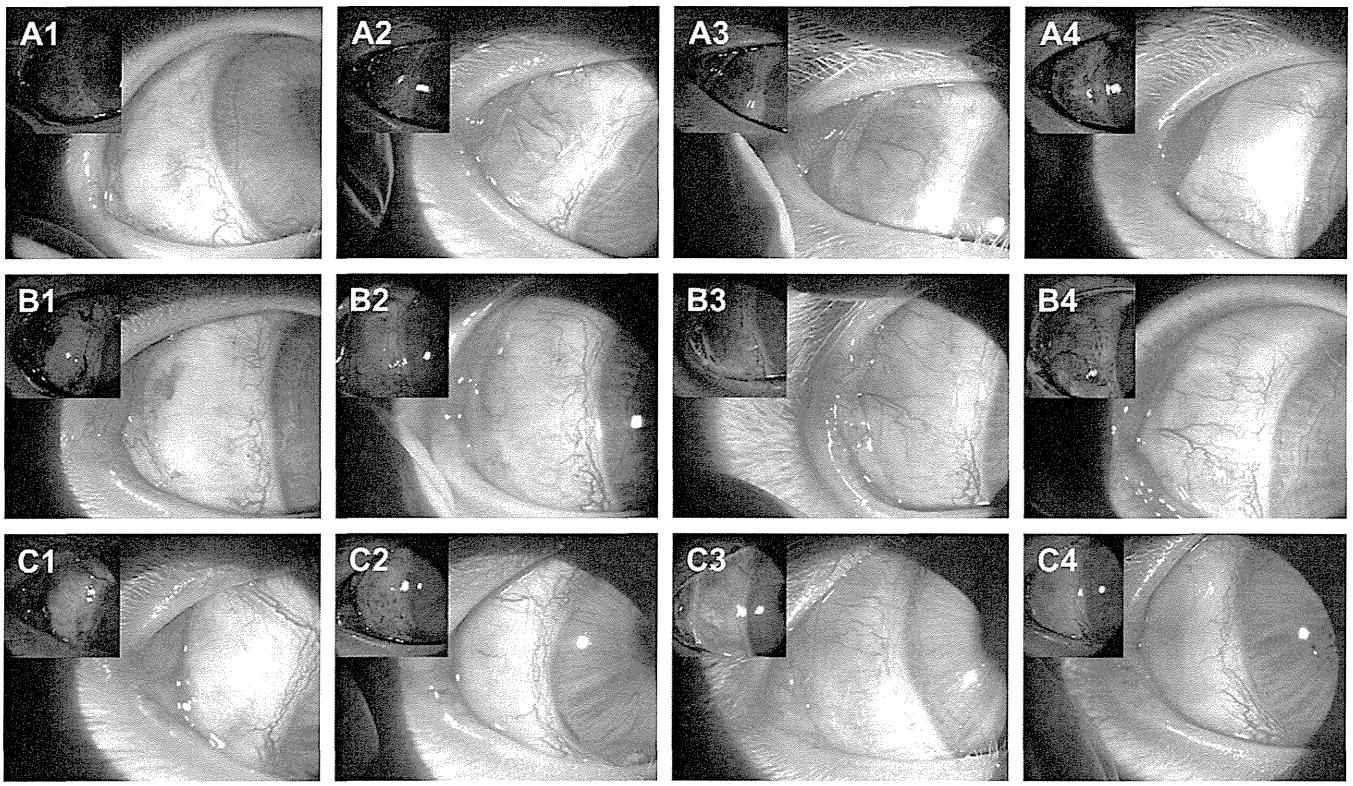

Fig. 4. Representative slit-lamp photographs of rabbits taken 2 (A1–C1), 4 (A2–C2), 8 (A3–C3), and 12 (A4–C4) weeks after sutureless transplantation with bioadhesive (A1–A4), conventional AMT (B1–B4), and no graft (C1–C4). Though the bare sclera without AM transplantation failed to epithelialize within 2 weeks (C1), the surface of AM (A1 and B1) was completely covered with epithelium at 2 weeks after transplantation. The covered epithelium on AM was stable and there was no significant difference between sutureless AMT and conventional AMT eyes in regards to hyperemia (A and B).

histologically, ultrastructurally, and immunohistochemically examined on the 12-week samples.

2.5. Electron microscopic examination

2.5.1. Transmission electron microscopy

Samples were fixed in 2.5% glutaraldehyde in PBS buffer prior to processing for transmission electron microscopy. They were dissected into small pieces and washed three times in PBS for 15 min. Samples were post-fixed in 2% osmium tetroxide for 2 h and washed again in PBS before being passed through a graded ethanol series. Specimens were then transferred to propylene oxide twice for 20 min each time. They were placed in a solution containing 50% propylene oxide and 50% Araldite resin (Agar Scientific, Stansted, Essex, UK) overnight after which they were transferred to 100% resin and infiltrated overnight under agitation. The samples were embedded in moulds containing fresh resin and polymerized at 60 °C for 24–36 h. Ultra-thin sections (50–70 nm thick) were cut on a microtome (Ultracut E; Reichert, Depew, NY, USA), collected on naked copper grids and counterstained prior to examination on a transmission electron microscope (JEM 1010; JEOL Ltd., Tokyo, Japan).

2.5.2. Scanning electron microscopy

Samples were fixed in 2.5% glutaraldehyde in PBS buffer prior to processing for transmission electron microscopy. They were dissected into small pieces and washed three times in PBS for 15 min. Samples were post-fixed in 2% osmium tetroxide for 2 h and washed again in PBS before being passed through a graded ethanol series. Samples were then transferred to hexamethyldisilazane (HMDS) for 20 min then air-dried. The samples were then mounted on aluminum stubs and sputter coated with gold using an S150A sputter coater (Edwards, Crawley, West Sussex, UK). Samples were examined on a scanning electron microscope (JSM 5600; JEOL Ltd., Tokyo, Japan).

2.6. Immunohistochemistry

Immunohistochemical studies were performed on three groups of the samples at 12 weeks after operation using our previously described method [40]. Briefly, semi-thin (8 μm) cryostat sections were obtained from unfixed tissue embedded in Tissue-Tek® OCT compound. After fixing with cold acetone for 10 min, the sections were incubated with 1% bovine serum albumin for 30 min. Subsequently, the sections were incubated at RT for 1 h with the primary antibody (Table 1) and washed

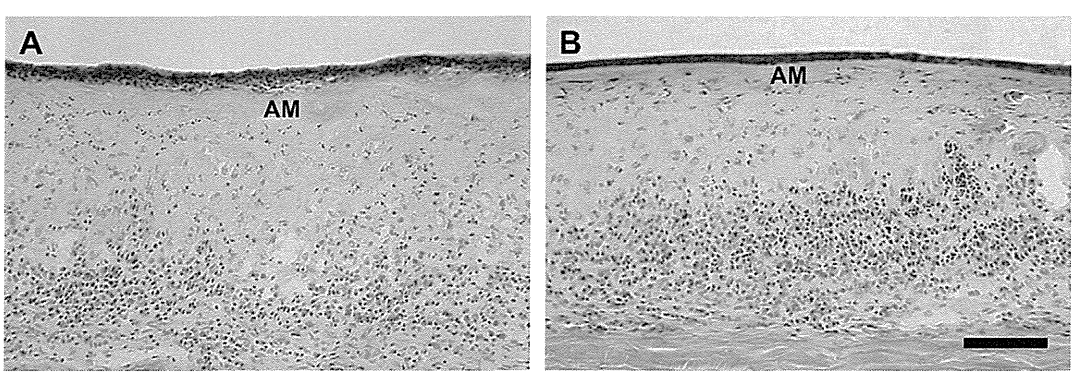

Fig. 5. Representative H&E staining for cryosections of the sutureless (A) and sutured (B) AMT models at 12 weeks after surgery. The transplanted membranes adapted well to the host scleral surface and migrating conjunctival epithelium on AM were well stratified and differentiated. Inflammatory cells were accumulated beneath both AMs, however, there were no significant differences between suture and non-suture models regarding the inflammatory reactions. Scale bar: 50 μm. AM: amniotic membrane.

three times in PBS containing 0.15% Triton X-100 (PBST) for 10 min. In the negative controls we replaced the primary antibody with the appropriate non-immune IgG. The sections were then incubated at RT for 1 h with appropriate secondary antibodies; Alexa Fluor 488 conjugated anti-mouse IgG antibody (Molecular Probes Inc., Eugene, OR, USA). After several washings with PBS, the sections were coverslipped using anti-fading mounting medium containing propidium iodide (Vectashield; Vector, Burlingame, CA, USA) and examined by confocal microscopy (TCS-SP2; Leica, Tokyo, Japan).

3. Results

3.1. Biocompatibility of CDB

In vitro cytotoxicity tests of aldehyded dextran and poly(L-lysine) indicated quite a low toxicity of both CDB components. However, due to the difficulty in cytotoxic evaluation of hydrogel materials *in vitro*, an *in vivo* toxicity test of the gelation sample was carried out using the rabbit subconjunctival injection model. Just after the injection, it was possible to identify the CDB beneath the conjunctiva due to its light blue color as seen through the translucent conjunctiva (Fig. 2A). The CDB is characterized by its self-degradability, and is known to gradually turn brown as it degrades. The ocular surface was expected to look brown had the CDB remained in that area, however, we were unable to find any brown discoloration under the conjunctiva at 4 weeks after the injection (Fig. 2B). Histological examination showed no apparent inflammation or scarring (Fig. 2C), and immunohistochemical findings in the conjunctival epithelial cells showed positive expressions of keratins 4 and 13 and mucin type 5AC (MUC5AC) (Fig. 2D–F), which are all expressed in normal conjunctival epithelial cells [41].

3.2. Sutureless transplantation

Cryopreserved AM was successfully transplanted onto the bare rabbit sclera without sutures as shown in Fig. 3A–D. The secured AMs had been fixed without loss or dislocation for 12 weeks. The grade of epithelialization and hyperemia in the surgical area was evaluated by slit lamp microscopy, with and without fluorescein (Fig. 4). Although the bare sclera without AMT was not epithelialized within 2 weeks, the color surface was covered within 2 weeks after sutured and sutureless AMT (Fig. 4A1, B1, C1). In regard to the hyperemia, there was no significant difference between suture models and non-suture models (Fig. 4A and B). The conjunctival fornix in the vicinity of the transplanted area was shortened only in the eyes that received simple recession of the conjunctiva (Fig. 4C), while it was sufficiently deep in the eyes with conventional and sutureless AMT (Fig. 4A and B).

3.3. Histological examination

Histological examinations of the 12-week samples of the suture and non-suture models showed that the transplanted membranes adapted well to the host scleral surface and that the migrating conjunctival epitheliums on the AM of both model types were well stratified and differentiated. It also showed that the inflammatory cells were accumulated beneath the AM in both models, however, there were no significant differences between the suture and non-suture models in regard to inflammatory reactions (Fig. 5).

3.4. Electron microscopic examination

The stromal side of the AM was coated with the CDB by dropping the solution onto the AM and then allowing a sufficient amount of elapsed time for the surface to dry. Scanning electron microscopic examination of the CDB-coated side of the AM showed a smooth surface that was relatively featureless (Fig. 6A). Transmission electron microscopic investigation of the AMT after 1 day showed a firm attachment of the AM to the sclera (Fig. 6B).

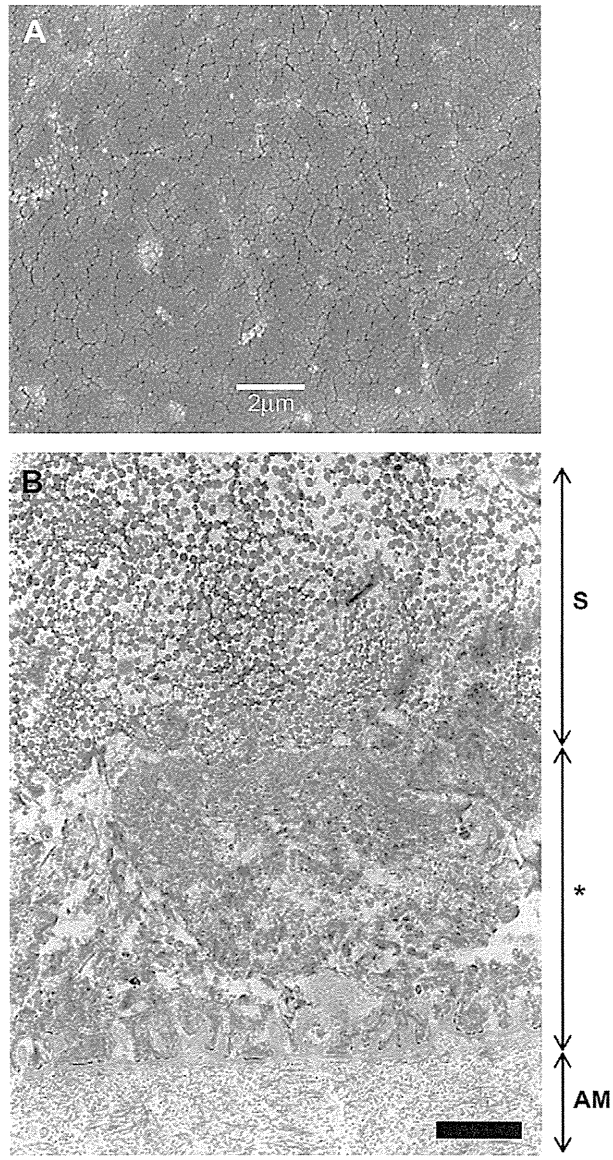

Fig. 6. Scanning electron microscopic investigation revealed that AM was fully covered by the bioadhesives (A). Transmission electron microscopic investigation of the AMT after 1 day showed a firm attachment of the AM to the sclera (B). Scale bars: 2 μm. S: sclera, asterisk: CDB.

3.5. Morphological findings of the conjunctival epithelial cells on AM

Scanning electron microscopic examination of the conjunctival epithelial cells on the AM after sutureless AMT showed a continuous layer of normal looking flat, irregular-shaped polygonal cells. The cells appeared completely normal since they had distinct borders and their surfaces were covered with microvilli (Fig. 7A and B). Examination of the conjunctival epithelial cells by transmission electron microscopy showed normal looking cells forming 6–7 layers, from basal cells to wing and superficial cells, with neighboring cells having numerous desmosomal cell junctions (Fig. 7C and D). These cells were also well attached to the AM through frequent hemidesmosomal contacts (Fig. 7E and F).

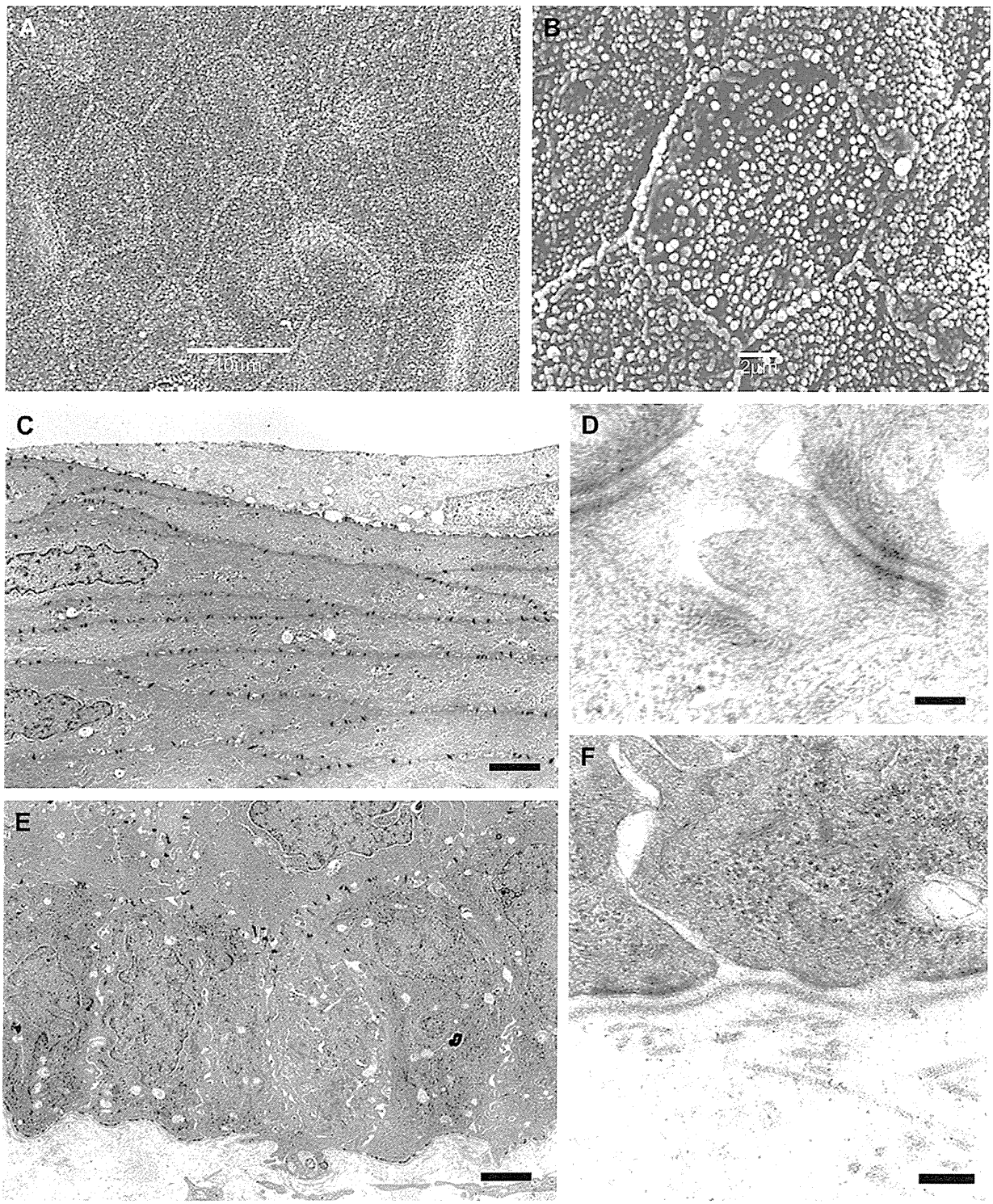

Fig. 7. Scanning electron microscopic examination of the conjunctival epithelial cells on the AM after sutureless AMT showed a continuous layer of normal looking flat irregular-shaped polygonal cells. The cells had distinct borders and their surfaces were covered with microvilli which they appeared completely normal (A and B). Examination of the conjunctival epithelial cells by transmission electron microscopy showed normal looking cells forming 6–7 layers, from basal cells to wing and superficial cells, with neighboring cells having numerous desmosomal cell junctions (C–E). These cells were also well attached to the AM through frequent hemidesmosomal contacts (F). Scale bars: (A) 10 μm, (B–D) 2 μm, (E and F) 100 nm.

3.6. Characterization of the conjunctival epithelial cells on AM

The characterization of the epithelial cells on three groups of samples was compared at 12 weeks by immunohistochemistry for cytokeratins (CK) (types 1, 4, 10, and 13), and MUC5AC (Fig. 8). The staining for CK4 and 13, and MUC5AC was detected at the epithelial cell layer on the slides from each group. There was no detectable staining for CK1 and 10. These staining patterns were similar to that of normal rabbit conjunctival epithelial cells [41].

4. Discussion

Many sutureless techniques have been previously developed using fibrin glue for ocular surface reconstruction [20,25–29,31,32],

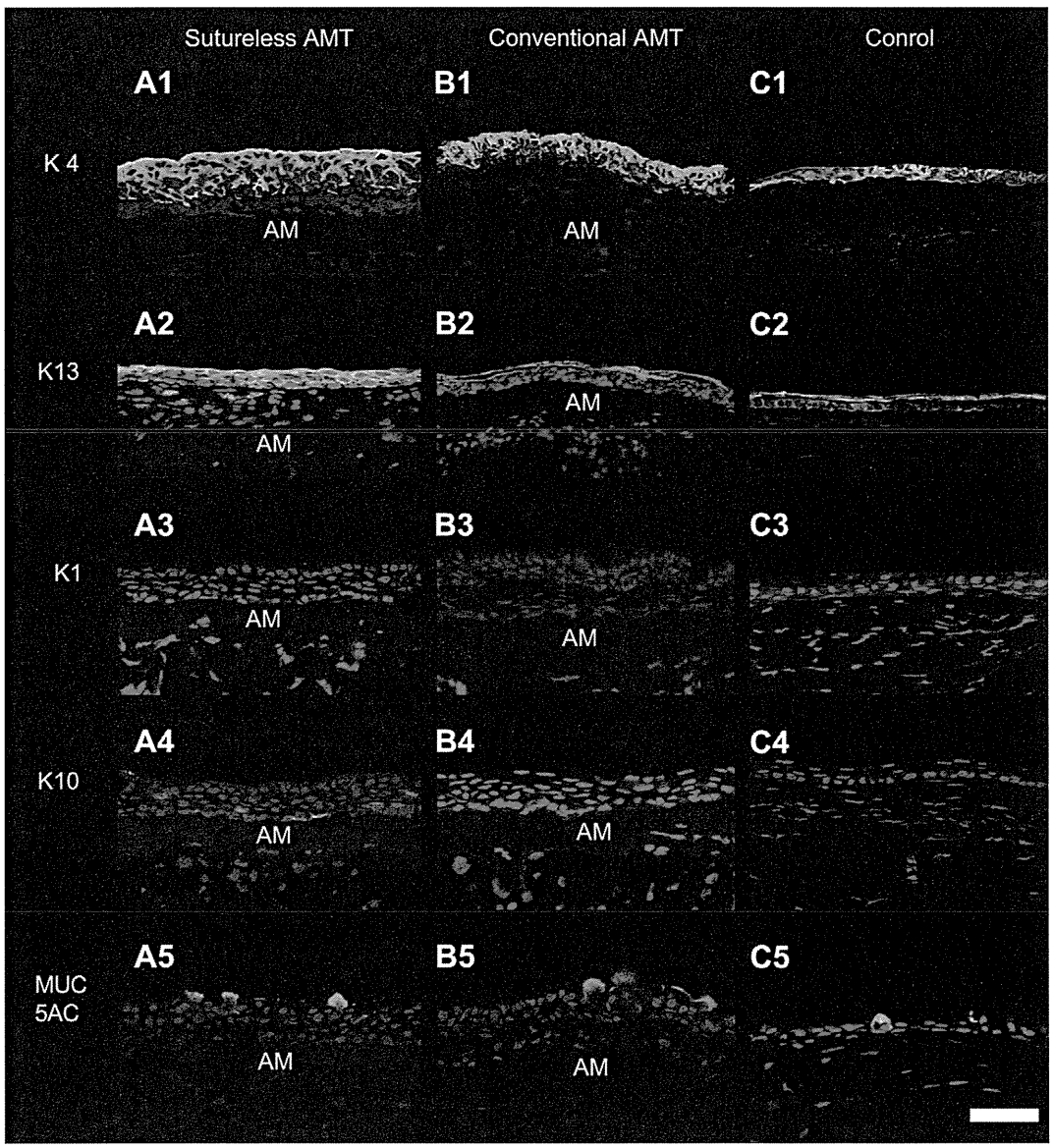

Fig. 8. Representative immunohistochemical staining of CK4, 13, 1, 10 and MUC5AC in sutureless AMT (A1–A5), conventional AMT (B1–B5) and no graft (control) (C1–C5). CK4, 13 and MUC5AC were expressed at the epithelial cell layer of sutureless AMT (A1, A2 and A5) and conventional AMT (B1, B2 and B5). In contrast, CK1 and 10 were not expressed in any of sutureless AMT (A3 and A4) and conventional AMT (B3 and B4). These staining patterns were similar to that of simple recession of conjunctiva (C1–C5). Scale bar: 50 μm.

however, the risk of disease transmission had come into question after the operations using fibrin glue [35–37]. To overcome that risk, we devised a sutureless transplantation using a newly developed bioadhesive that is chemically defined, self-degradable, and biocompatible with the ocular surface. To the best of our knowledge, this is the first attempt to apply a chemically defined adhesive that is strong, safe, biocompatible, and biodegradable for ocular surface reconstruction.

Many tissue adhesives have been improved to overcome the problems that are encountered with sutures. Cyanoacrylates are one of the synthetic adhesives that have traditionally been applied to ocular surfaces since the 1960s for the repair of corneal perforations [42]. They have also been used successfully for cataract wound closure [43], leaking blebs [44], and conjunctival wound closure [45]. However, chronic inflammation and delay of wound healing have occurred because of their toxicity [46], and thereby they are far from safe for the ocular surface. Other disadvantages have also been previously reported related to its inflexibility, inability to be reabsorbed, and lack of transparency [47]. Recently, synthetic and non-biologic adhesives have been developed such as biodendrimer [48], hydrogel adhesives [49], and chondroitin sulfate aldehydes [50], for ocular surface. They have been shown to be effective for sealing corneal incisions, however, in regard to toxicity, biocompatibility, and biodegradability, they have yet to be fully examined.

To perform sutureless AMT successfully, it is essential that the adhesive can be easily handled. The adhesive in this report was easy to handle for sutureless AMT without unexpected gelatinization or a complicated technique. Immediately after exiting the syringe, our newly devised, liquid-form CDB was properly spread on the ocular surface, gradually gelatinized, and then finally fixed the AM firmly onto the ocular surface for a long time. The CDB had a smooth rubbery texture when gelled and showed sufficient flexibility even after becoming totally gelled. Moreover, and adding to the effectiveness of this new adhesive, the gel formation time can be altered so that operators can match an appropriate gel formation time to the required handling time.

Previously synthesized adhesives have been associated with problems such as chronic inflammation and delayed wound healing due to their residual toxicity and degradation properties. Our

new CDB has already shown to be of low cytotoxicity *in vitro*, and moreover, it degraded into the surrounding tissue within 4 weeks, with no additional inflammation and no influence on the character of keratin and MUC5AC expression in nearby conjunctiva. These findings indicate that the CDB is sufficiently biocompatible and biodegradable for use on the ocular surface.

We successfully performed the sutureless AMT with this adhesive on rabbit sclera. Histological and electron microscopic examination showed that the AM was firmly attached to the sclera, and slit lamp examination also showed good fixation without loss or dislocation for at least 3 months. For a firm attachment, stable crosslinking between the molecules is needed. The formation of Schiff base strongly depends on the solution pH, with a higher pH enhancing the reaction. However, the solution pH of aldehyded dextran and poly(L-lysine) are around 5 and 9, respectively, and the pH of the mixture is approximately 7 (neutral). High reactivity of poly(L-lysine) might cause the effective gel formation even at the neutral pH (data not shown). Although we did not exactly show whether the crosslinkings with the Schiff base was modified *in vivo* or not, the fixation on the ocular surface lasted at least 3 months. The period of epithelialization and degree of hyperemia in eyes with sutureless AMT were similar to those associated with sutured AM, and both methods revealed prompt epithelialization when compared to non-transplanted eyes. These findings show that our sutureless AMT technique using CDB is equally effective and useful for ocular surface reconstructions.

When bioadhesives are applied for sutureless AMT, what is of key importance is that they are non-toxic and thus have little influence on the surrounding tissues, especially on conjunctival epithelial cells. In this study, the ultrastructure of conjunctival epithelial cells on the transplanted AM showed the normal features of conjunctiva. On the surface, hexagonal cells had regular microvillis and were closely attached to neighboring cells with numerous desmosomal cell junctions, and in the basal layers had frequent hemidesmosomal contacts to the AM. These findings are compatible to the previous report that AM has been shown to promote a predominantly conjunctival non-goblet epithelial phenotype with expression of microvilli, intercellular junction, and increased density of desmosomes and hemidesmosomes [51]. We did not exactly compare the ultrastructural feature to either the sutured model or normal conjunctiva, however, the conjunctiva on the AM was at least similar to normal even in the presence of CDB nearby. Furthermore, the epithelium expressed CK4 and 13, which is specific for conjunctival epithelium, and did not express keratinized marker K1 or 10, thus indicating that the CDB did not affect normal differentiation of the conjunctival epithelial cells. Taken together, these results suggest that the CDB has no, or if any, very little negative influence on surrounding tissues and is sufficiently safe for use on the ocular surface.

This study has shown that our newly devised CDB is safe and useful for sutureless AMT. Based on our results, we expect the CDB to be applied in a variety of sutureless operations on the ocular surface including conjunctival closure after several kinds of operations, cultivated corneal or oral mucosal epithelium transplantation, and lamellar keratoplasty. We are currently in the process of investigating a variety of applications.

5. Conclusions

Our study demonstrates a safe and simple technique for sutureless AMT using a chemically defined bioadhesive which promotes a secure and rapid adhesion onto the sclera *in vivo* without the need for suturing. If this technique is applied for human ocular surface reconstruction, we expect it to achieve safe and satisfactory results while simultaneously reducing postoperative pain and discomfort. Further investigation is still needed for its clinical use.

Acknowledgments

We thank Mr. J. Bush for editing our manuscript, and Ms. Saito and Horikiri for preparing the AM. This study was supported in part by Grants-in-Aid for scientific research from the Japanese Ministry of Health, Labor and Welfare (H16–Saisei-007), and the Japanese Ministry of Education, Culture, Sports, Science and Technology (Kobe Translational Research Cluster), a research grant from the Kyoto Foundation for the Promotion of Medical Science, the Intramural Research Fund of Kyoto Prefectural University of Medicine, and BBSRC in UK.

References

[1] Kim JS, Kim JC, Na BK, Jeong JM, Song CY. Amniotic membrane patching promotes healing and inhibits proteinase activity on wound healing following acute corneal alkali burn. Exp Eye Res 2000;70(3):329–37.
[2] Solomon A, Rosenblatt M, Monroy D, Ji Z, Pflugfelder SC, Tseng SCG. Suppression of interleukin 1α and interleukin 1β in human limbal epithelial cells cultured on the amniotic membrane stromal matrix. Br J Ophthalmol 2001; 85(4):444–9.
[3] Tseng SC, Li DQ, Ma X. Suppression of transforming growth factor-beta isoforms, TGF-β receptor type II, and myofibroblast differentiation in cultured human corneal and limbal fibroblasts by amniotic membrane matrix. J Cell Physiol 1999;179(3):325–35.
[4] Talmi YP, Sigler L, Inge E, Finkelstein Y, Zohar Y. Antibacterial properties of human amniotic membranes. Placenta 1991;12(3):285–8.
[5] Hao Y, Ma DH, Hwang DG, Kim WS, Zhang F. Identification of antiangiogenic and antiinflammatory proteins in human amniotic membrane. Cornea 2000; 19(3):348–52.
[6] Tseng SC, Prabhasawat P, Lee SH. Amniotic membrane transplantation for conjunctival surface reconstruction. Am J Ophthalmol 1997;124(6):765–74.
[7] Fernandes M, Sridhar MS, Sangwan VS, Rao GN. Amniotic membrane transplantation for ocular surface reconstruction. Cornea 2005;24(6):643–53.
[8] Koizumi NJ, Inatomi TJ, Sotozono CJ, Fullwood NJ, Quantock AJ, Kinoshita S. Growth factor mRNA and protein in preserved human amniotic membrane. Curr Eye Res 2000;20(3):173–7.
[9] Kim JC, Tseng SC. Transplantation of preserved human amniotic membrane for surface reconstruction in severely damaged rabbit corneas. Cornea 1995; 14(5):473–84.
[10] Lee SH, Tseng SC. Amniotic membrane transplantation for persistent epithelial defects with ulceration. Am J Ophthalmol 1997;123(3):303–12.
[11] Letko E, Stechschulte SU, Kenyon KR, Sadeq N, Romero TR, Samson CM, et al. Amniotic membrane inlay and overlay grafting for corneal epithelial defects and stromal ulcers. Arch Ophthalmol 2001;119(5):659–63.
[12] Solomon A, Pires RT, Tseng SC. Amniotic membrane transplantation after extensive removal of primary and recurrent pterygia. Ophthalmology 2001; 108(3):449–60.
[13] Tsubota K, Satake Y, Ohyama M, Toda I, Takano Y, Ono M, et al. Surgical reconstruction of the ocular surface in advanced ocular cicatricial pemphigoid and Stevens–Johnson syndrome. Am J Ophthalmol 1996;122(1): 38–52.
[14] Honavar SG, Bansal AK, Sangwan VS, Rao GN. Amniotic membrane transplantation for ocular surface reconstruction in Stevens–Johnson syndrome. Ophthalmology 2000;107(5):975–9.
[15] Tsai RJ-F, Li L-M, Chen J-K. Reconstruction of damaged corneas by transplantation of autologous limbal epithelial cells. N Engl J Med 2000;343(2): 86–93.
[16] Tseng SCG, Prabhasawat P, Barton K, Gray T, Meller D. Amniotic membrane transplantation with or without limbal allografts for corneal surface reconstruction in patients with limbal stem cell deficiency. Arch Ophthalmol 1998;116(4):431–41.
[17] Meallet MA, Espana EM, Grueterich M, Ti SE, Goto E, Tseng SC. Amniotic membrane transplantation with conjunctival limbal autograft for total limbal stem cell deficiency. Ophthalmology 2003;110(8):1585–92.
[18] Tsubota K, Satake Y, Kaido M, Shinozaki N, Shimmura S, Bissen-Miyajima H, et al. Treatment of severe ocular-surface disorders with corneal epithelial stem-cell transplantation. N Engl J Med 1999;340(22):1697–703.
[19] Azuara-Blanco A, Pillai CT, Dua HS. Amniotic membrane transplantation for ocular surface reconstruction. Br J Ophthalmol 1999;83(4):399–402.
[20] Uy HS, Reyes JM, Flores JD, Lim-Bon-Siong R. Comparison of fibrin glue and sutures for attaching conjunctival autografts after pterygium excision. Ophthalmology 2005;112(4):667–71.
[21] Leahey AB, Avery RL, Gottsch JD, Mallette RA, Stark WJ. Suture abscesses after penetrating keratoplasty. Cornea 1993;12(6):489–92.
[22] Cameron JA, Huaman A. Corneoscleral abscess resulting from a broken suture after cataract surgery. J Cataract Refract Surg 1994;20(1):82–3.

[23] Starck T, Kenyon KR, Serrano F. Conjunctival autograft for primary and recurrent pterygia: surgical technique and problem management. Cornea 1991; 10(3):196–202.
[24] Soong HK, Kenyon KR. Adverse reactions to virgin silk sutures in cataract surgery. Ophthalmology 1984;91(5):479–83.
[25] Zauberman H, Hemo I. Use of fibrin glue in ocular surgery. Ophthalmic Surg 1988;19(2):132–3.
[26] Dadeya S, Ms K. Strabismus surgery: fibrin glue versus vicryl for conjunctival closure. Acta Ophthalmol Scand 2001;79(5):515–7.
[27] Cohen RA, McDonald MB. Fixation of conjunctival autografts with an organic tissue adhesive. Arch Ophthalmol 1993;111(9):1167–8.
[28] Koranyi G, Seregard S, Kopp ED. Cut and paste: a no suture, small incision approach to pterygium surgery. Br J Ophthalmol 2004;88(7):911–4.
[29] Pfister RR, Sommers CI. Fibrin sealant in corneal stem cell transplantation. Cornea 2005;24(5):593–8.
[30] Nishida K, Yamato M, Hayashida Y, Watanabe K, Maeda N, Watanabe H, et al. Functional bioengineered corneal epithelial sheet grafts from corneal stem cells expanded ex vivo on a temperature-responsive cell culture surface. Transplantation 2004;77(3):379–85.
[31] Kaufman HE, Insler MS, Ibrahim-Elzembely HA, Kaufman SC. Human fibrin tissue adhesive for sutureless lamellar keratoplasty and scleral patch adhesion: a pilot study. Ophthalmology 2003;110(11):2168–72.
[32] Kheirkhah A, Casas V, Blanco G, Li W, Hayashida Y, Chen YT, et al. Amniotic membrane transplantation with fibrin glue for conjunctivochalasis. Am J Ophthalmol 2007;144(2):311–3.
[33] Sekiyama E, Nakamura T, Kurihara E, Cooper LJ, Fullwood NJ, Takaoka M, et al. Novel sutureless transplantation of bioadhesive-coated, freeze-dried amniotic membrane for ocular surface reconstruction. Invest Ophthalmol Vis Sci 2007; 48(4):1528–34.
[34] Nakamura T, Yoshitani M, Rigby H, Fullwood NJ, Ito W, Inatomi T, et al. Sterilized, freeze-dried amniotic membrane: a useful substrate for ocular surface reconstruction. Invest Ophthalmol Vis Sci 2004;45(1):93–9.
[35] Hino M, Ishiko O, Honda KI, Yamane T, Ohta K, Takubo T, et al. Transmission of symptomatic parvovirus B19 infection by fibrin sealant used during surgery. Br J Haematol 2000;108(1):194–5.
[36] Kawamura M, Sawafuji M, Watanabe M, Horinouchi H, Kobayashi K. Frequency of transmission of human parvovirus B19 infection by fibrin sealant used during thoracic surgery. Ann Thorac Surg 2002;73(4):1098–100.
[37] Taylor DM. Inactivation of TSE agents: safety of blood and blood-derived products. Transfus Clin Biol 2003;10(1):23–5.
[38] Nakajima N, Sugai H, Tsutsmi S, Hyon S-H. Self-degradable bioadhesive. Key Eng Mater 2007;342–343:713–6.
[39] Koizumi N, Inatomi T, Quantock AJ, Fullwood NJ, Dota A, Kinoshita S. Amniotic membrane as a substrate for cultivating limbal corneal epithelial cells for autologous transplantation in rabbits. Cornea 2000;19(1):65–71.
[40] Takaoka M, Nakamura T, Ban Y, Kinoshita S. Phenotypic investigation of cell junction-related proteins in gelatinous drop-like corneal dystrophy. Invest Ophthalmol Vis Sci 2007;48(3):1095–101.
[41] Nakamura T, Endo K, Cooper LJ, Fullwood NJ, Tanifuji N, Tsuzuki M, et al. The successful culture and autologous transplantation of rabbit oral mucosal epithelial cells on amniotic membrane. Invest Ophthalmol Vis Sci 2003;44(1): 106–16.
[42] Webster Jr RG, Slansky HH, Refojo MF, Boruchoff SA, Dohlman CH. The use of adhesive for the closure of corneal perforations. Report of two cases. Arch Ophthalmol 1968;80(6):705–9.
[43] Price Jr JA, Wadsworth JA. Evaluation of an adhesive in cataract wound closure. Am J Ophthalmol 1969;68(4):663–8.
[44] Awan KJ, Spaeth PG. Use of isobutyl-2-cyanoacrylate tissue adhesive in the repair of conjunctival fistula in filtering procedures for glaucoma. Ann Ophthalmol 1974;6(8):851–3.
[45] Alio JL, Gomez J, Mulet E, Bujanda MM, Martinez JM, Molina Y. A new acrylic tissue adhesive for conjunctival surgery: experimental study. Ophthalmic Res 2003;35(6):306–12.
[46] Tseng YC, Tabata Y, Hyon SH, Ikada Y. In vitro toxicity test of 2-cyanoacrylate polymers by cell culture method. J Biomed Mater Res 1990;24(10): 1355–67.
[47] Bhatia SS. Ocular surface sealants and adhesives. Ocul Surf 2006;4(3): 146–54.
[48] Velazquez AJ, Carnahan MA, Kristinsson J, Stinnett S, Grinstaff MW, Kim T. New dendritic adhesives for sutureless ophthalmic surgical procedures: in vitro studies of corneal laceration repair. Arch Ophthalmol 2004;122(6): 867–70.
[49] Kalayci D, Fukuchi T, Edelman PG, Sawhney AS, Mehta MC, Hirose T. Hydrogel tissue adhesive for sealing corneal incisions. Ophthalmic Res 2003;35(3): 173–6.
[50] Reyes JM, Herretes S, Pirouzmanesh A, Wang DA, Elisseeff JH, Jun A, et al. A modified chondroitin sulfate aldehyde adhesive for sealing corneal incisions. Invest Ophthalmol Vis Sci 2005;46(4):1247–50.
[51] Meller D, Tseng SC. Conjunctival epithelial cell differentiation on amniotic membrane. Invest Ophthalmol Vis Sci 1999;40(5):878–86.

Rheology of Tear Film Lipid Layer Spread in Normal and Aqueous Tear–Deficient Dry Eyes

Norihiko Yokoi,[1] *Hideaki Yamada,*[1] *Yutaka Mizukusa,*[2] *Anthony J. Bron,*[3] *John M. Tiffany,*[3] *Takahisa Kato,*[4] *and Shigeru Kinoshita*[1]

Purpose. To analyze the relationship between tear volume and tear film lipid layer (TFLL) spread.

Methods. Twenty-nine eyes from 22 subjects, including normal eyes and eyes with aqueous tear-deficient dry eye, were enrolled in this study. In all eyes, the radius of curvature (*R*: mm) of the central lower tear meniscus was measured with a videomeniscometer, and interference images from the TFLL were recorded with a video-interferometer. Interference images were captured as still images every 0.05 second, and the relationship between the acquisition time for each image after a blink and the averaged heights of the spreading TFLL in the upstroke of the blink were calculated.

Results. In all cases, the time-dependent changes in TFLL spread could be described by the expression $H(t) - H(0) = \rho[1 - \exp(-t/\lambda)]$, where $H(t)$ is the averaged height in millimeters at time t, $H(0)$ is the averaged height at $t = 0$, ρ is a constant, t is time in seconds, and λ is the characteristic time in seconds. A statistically significant correlation was found between those changes and the initial upward velocity of the spreading TFLL [$H'(0) = dH(0)/dt$] and R ($r = 0.573$; $P = 0.003$).

Conclusions. This study demonstrated that the time-dependent changes of TFLL spread are compatible with the Voigt model of viscoelasticity and that the initial velocity of TFLL spread after a blink decreased in proportion to the decrease of tear volume. There is potential interest in using this parameter to diagnose and evaluate the severity of aqueous tear deficiency. (*Invest Ophthalmol Vis Sci.* 2008;49:5319–5324) DOI:10.1167/iovs.07-1407

The aqueous layer of the tear film is covered by a thin lipid layer[1] that can be imaged noninvasively by interferometry.[2–4] We have reported elsewhere that graded interference patterns can be used as a parameter to screen dry eye and evaluate its severity.[5] Other studies have shown that after a blink, the tear film lipid layer (TFLL) spreads over the aqueous layer in a reproducible manner[2,6–9] and that its dynamics can be observed using an interferometer. Such studies[10,11] have noted that the time taken for the interference pattern to stabilize after a blink (defined as spreading time) is longer in aqueous-deficient dry eyes than in aqueous-sufficient normal eyes. Goto and Tseng[11] noted that the spreading time was shortened in aqueous tear-deficient dry eyes after punctal occlusion and proposed that spreading is affected by aqueous tear volume. This semiquantitative method offers a novel direct approach to the study of lipid-layer kinetics. A related report has analyzed the kinetic behavior of particles embedded in the tear film, probably located at the level of the TFLL.[12,13]

With the use of our interferometer, we found that in the upstroke of the blink, the speed of upward spread of the TFLL slows dramatically to reach a stable position in the normal eye, within approximately 1 second. This has also been observed by other authors.[9,11,12] This effect can be seen more clearly in eyes with aqueous tear deficiency because the speed of spreading is slower.

We hypothesized that this time-dependent behavior might reflect a viscoelastic property of the tear film. With this in mind, we conducted a study of TFLL dynamics. In addition, we were interested in the relationship between the TFLL spread and tear volume.

Subjects and Methods

Subjects

Twenty-nine eyes from 22 subjects (1 eye from 1 man and 28 eyes from 21 women) were enrolled in this study. The age of the subjects ranged from 42 to 87 years (64.6 ± 11.0 years; mean ± SD). According to the diagnostic criteria given below, there were 5 normal eyes of 4 healthy subjects (54.8 ± 4.7 years) and 24 aqueous tear-deficient dry eyes of 18 patients (66.8 ± 10.9 years). Of the 24 aqueous tear-deficient dry eyes, 15 eyes were from 11 patients with Sjögren's-syndrome dry eye (SSDE), and 9 eyes were from 7 patients with non-Sjögren's-syndrome dry eye (NSDE).[14]

Tear tests were performed on all subjects before enrollment. These included the Schirmer I test[15] (abnormal value, ≤5 mm/5 min), the measurement of fluorescein break-up time (BUT)[16] (abnormal value, ≤5 seconds), and the grading of corneal staining with fluorescein[17] and of ocular surface staining with rose Bengal.[18] Abnormal scores for fluorescein were A1D1 and greater; A and D representing area and density, respectively, were graded from 0 to 1 (mild), 2 (moderate), and 3 (severe). An abnormal score for rose Bengal, based on the van Bijsterveld criteria, was ≥3.

The aqueous tear-deficient dry eyes enrolled in the study met the inclusion criteria, among those being at least one abnormal Schirmer I test value and abnormal scores for either fluorescein or rose Bengal staining. All eyes also showed abnormal BUT values. Patients with aqueous tear-deficient dry eye were categorized as SSDE or NSDE, with the diagnosis of SSDE based on the criteria of Fox et al.[19] Healthy eyes in this study met the following criteria: normal Schirmer I test value, normal scores for fluorescein and rose Bengal staining, and normal BUT values. Exclusion criteria were meibomian gland dysfunction, punctal-plug occlusion or surgical punctal occlusion, previous corneal surgery, previous or current corneal disease (excluding aqueous tear-deficient dry eye), and hard or soft contact lens wear by the subject.

From the [1]Department of Ophthalmology, Kyoto Prefectural University of Medicine, Kyoto, Japan; the [2]Kowa Co., Ltd., Tokyo, Japan; the [3]Nuffield Laboratory of Ophthalmology, University of Oxford, Oxford, United Kingdom; and the [4]Department of Mechanical Engineering, University of Tokyo, Tokyo, Japan.

Supported by Grant-in-Aid 19592034 for Scientific Research from the Ministry of Education, Science, Culture, and Sports of Japan.

Submitted for publication October 31, 2007; revised March 28 and April 21, 2008; accepted October 14, 2008.

Disclosure: **N. Yokoi**, None; **H. Yamada**, None; **Y. Mizukusa**, None; **A.J. Bron**, None; **J.M. Tiffany**, None; **T. Kato**, None; **S. Kinoshita**, None

The publication costs of this article were defrayed in part by page charge payment. This article must therefore be marked "*advertisement*" in accordance with 18 U.S.C. §1734 solely to indicate this fact.

Corresponding author: Norihiko Yokoi, Department of Ophthalmology, Kyoto Prefectural University of Medicine, 465 Kajii-cho, Hirokoji-agaru, Kawaramachi-dori, Kamigyo-ku, Kyoto 602-0841, Japan; nyokoi@koto.kpu-m.ac.jp.

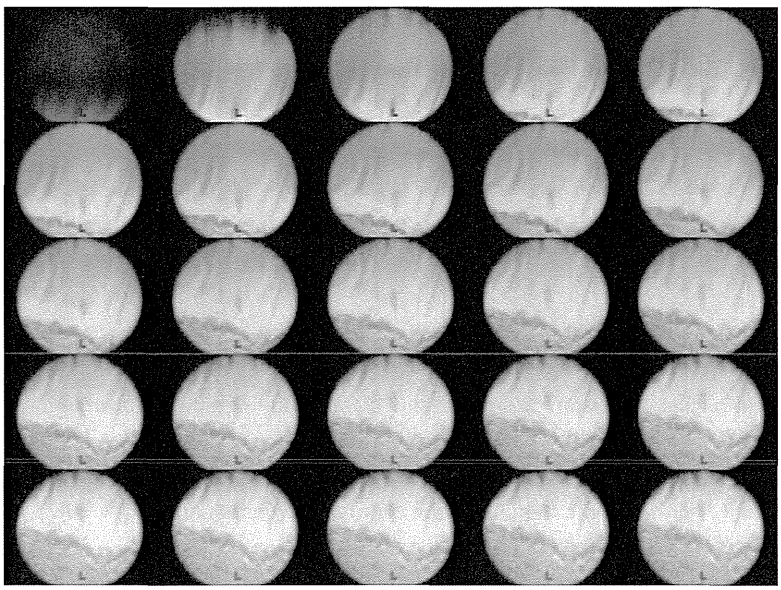

FIGURE 1. Representative sequential images of the spreading tear-film lipid layer, captured every 0.05 second after a blink (case 2).

In all subjects, reflected images from the central lower tear meniscus were first digitally recorded in the interblink period, during natural blinking with a video-meniscometer.[20-25] Immediately after that, interference images from the TFLL were digitally recorded just after a blink with a video-interferometer (DR-1; Kowa, Tokyo, Japan).[5,25]

This research was approved by the Committee for Ethical Issues on Human Research of Kyoto Prefectural University of Medicine (C-240) and followed the tenets of the Declaration of Helsinki. Informed consent was obtained from all dry eye patients and healthy subjects after explanation of the nature and possible consequences of participation in the study.

Evaluation of the Radius of the Lower Tear Meniscus Using the Video-Meniscometer

The radius of curvature (*R*: mm) of the tear meniscus at the central lower eyelid was measured by video-meniscometry.[20-25] With this, a real-time reflected image of a target consisting of a pair of horizontal, black-and-white stripes was captured digitally, and *R* was calculated using the concave mirror formula.[20-22] In our video-meniscometry, the *R* of the lower tear meniscus is measured as the average of three consecutive measurements (Sugita J, et al. *IOVS* 2002;43 ARVO E-Abstract 95). In the model, *R* is assumed to be constant over the duration of the interblink, as demonstrated by Palakuri et al.[26] for the upper and lower tear meniscus using optical coherence tomography. However, it should be noted that Johnson et al.,[27] using the video slit-lamp technique, reported an increase of *R* at the end of the interblink period. The tear meniscus is reportedly responsible for 75% to 90% of the total tear volume,[28] and the value of *R* reportedly reflects the total tear volume over the ocular surface.[23]

Rheologic Analysis of Interference Images from the Precorneal Tear Film Lipid Layer by Use of the Video-Interferometer

The video-interferometer (DR-1; Kowa) provides information about lipid layer thickness and lipid layer spread after a blink[5,10,11,24,25] and is equipped with low- and high-magnification viewing modes that allow observation of 7-mm and 2-mm circular areas in the central cornea, respectively.[24] In this study, the low-magnification mode was the primary mode selected to obtain information regarding the behavior of the precorneal TFLL.

Interference images obtained by the video-interferometer were recorded noninvasively, in real time, using a digital video recorder. Images were sequentially captured into a computer as still images every 0.05 second (Fig. 1) with the use of specially developed software. Regions of the spreading lipid layer after a blink were clipped along the delineated border using graphic software (Photoshop CS, version 8.0.1; Adobe Systems, San Jose, CA; Fig. 2). Given that only

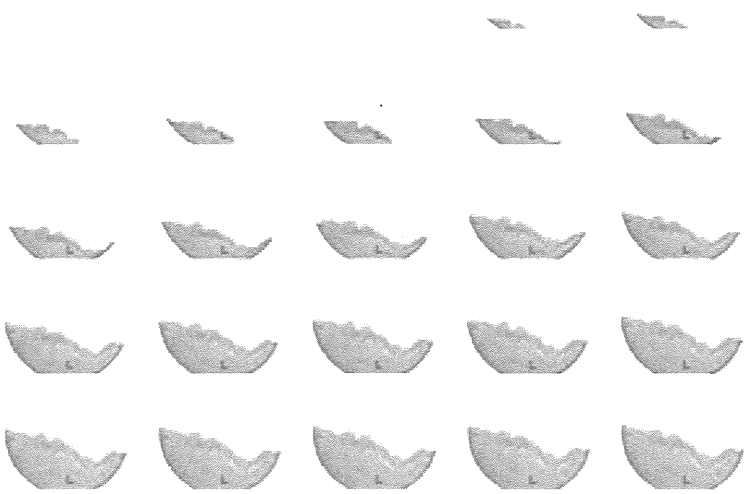

FIGURE 2. Regions of spreading lipid layer clipped along the border.

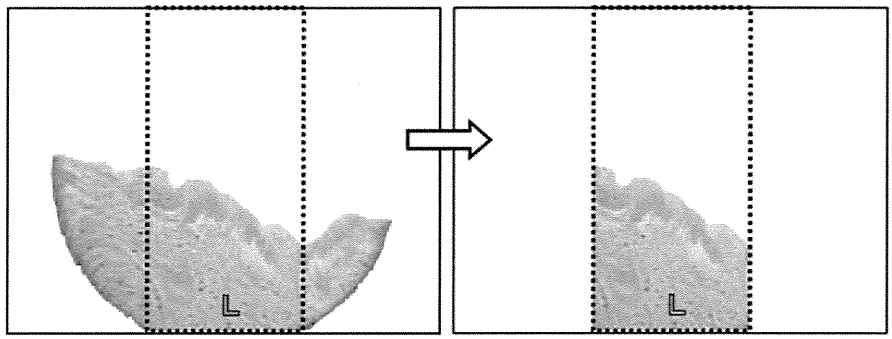

FIGURE 3. The central rectangular area (200 pixels horizontal × 480 pixels vertical) was cropped from the clipped spreading lipid image as the representative region for the whole tear-film lipid layer over the cornea and the averaged height of spreading lipid within the area were calculated.

upward spreading was considered and not the associated widening of the TFLL within the viewing window, only the area of lipid film within a rectangle 200 pixels (horizontal) × 480 pixels (vertical) was considered (Fig. 3). The averaged heights of each spreading lipid sheet within the rectangular areas were calculated using specially developed software that permitted averaging of the length of spreading lipid along the vertical y-direction at each pixel point along the horizontal x-direction within the rectangular area. Images of the spreading TFLLs with ill-delineated upper borders and images with no spreading pattern, possibly because of extremely severe aqueous tear deficiency, were excluded. After calculating the averaged heights of the spreading lipid, the relationship between the acquisition time for the images after a blink and the calculated averaged heights of the spreading lipid were plotted. Curve-fitting to the plots satisfied an exponential equation in keeping with the simple rheological model of Voigt[29] describing the behavior of a viscoelastic material (see Discussion).

In all 29 eyes studied, the relationship between the radius of the central lower tear meniscus (R: mm), which was proportional to the total tear volume over the ocular surface,[23] and the initial upward velocity of the lipid layer spread were analyzed. The Spearman correlation coefficient by rank test was performed, and $P \leq 0.05$ was considered statistically significant.

RESULTS

In all eyes, the time-dependent changes in H of lipid layer spread were found to conform to an exponential model of the form $H(t) - H(0) = \rho[1 - \exp(-t/\lambda)]$, where $H(t)$ is the averaged heights in millimeters at time t, $H(0)$ is the averaged heights at time $t = 0$, ρ is a constant, t is time in seconds, and λ is characteristic time in seconds.

One representative example (case 2, Table 1) of spreading behavior is shown in Figure 1. Curve-fitting to the representative three examples—including cases 1, 2, and 3 in Table 1—is shown in Figure 4. The constants of the exponential equations and corresponding R values calculated from the video-meniscometer-detected images (Fig. 5) from the central lower tear meniscus in three representative cases are given in Table 1.

The relationship between R and $H'(0)$ is shown in Figure 6. There was a statistically significant correlation between R and $H'(0)$ ($r = 0.573$; $P = 0.003$; Spearman correlation coefficient by rank test). The relationship between R and the other parameters, including $H(0)$, ρ, and λ, was also analyzed. As a result, a similar and statistically significant correlation was found between R and ρ ($r = 0.573$; $P = 0.002$), and a weak, statistically insignificant correlation was found between R and $H(0)$ ($r = 0.318$; $P = 0.095$). However, there was no statistically significant correlation between R and λ ($r = -0.241$; $P = 0.194$).

TABLE 1. Constants of the Exponential Equations and the Corresponding R

Case	$H(0)$ (mm)	ρ (mm)	λ (s)	R (mm)	$H'(0)$ (mm/s)
1	0.08	1.54	0.68	0.09	2.25
2	0.02	4.00	0.79	0.14	5.04
3	2.96	2.85	0.14	0.45	20.52

DISCUSSION

In this study, images of the spreading TFLL were obtained noninvasively[5,10,11,25] at intervals of 0.05 second, allowing the dynamics of the TFLL spread to be analyzed quantitatively. The time dependence of the averaged height of the spreading TFLL, as determined from the captured images, was successfully fitted to an exponential formula of the form $H(t) - H(0) = \rho[1 - \exp(-t/\lambda)]$, where $H(t)$ is the averaged height in millimeters at time t, $H(0)$ is the averaged height at time $t = 0$, ρ is a constant, t is time in seconds, and λ is characteristic time in seconds. For the averaged height, H is first measured when the TFLL first appears in the viewing window. True $H(0)$ is the point in time at which the TFLL front first crosses the lower boundary of the viewing window, so that $H(0)$ as recorded is not zero and has a positive value. The size of this depends on the rate of movement of the TFLL and is higher when the rate of TFLL movement is high rather than when it is low (Table 1).

One of the simplest models of linear viscoelasticity is the Kelvin-Voigt (commonly referred to as the Voigt) model.[29] The applied stress σ can be related to the shear γ through the sum of elastic and viscous forces such that

$$\sigma = \kappa\gamma + \eta d\gamma/dt \qquad (1)$$

where κ is the coefficient of elasticity and η is the coefficient of viscosity. The elastic response can be represented by a

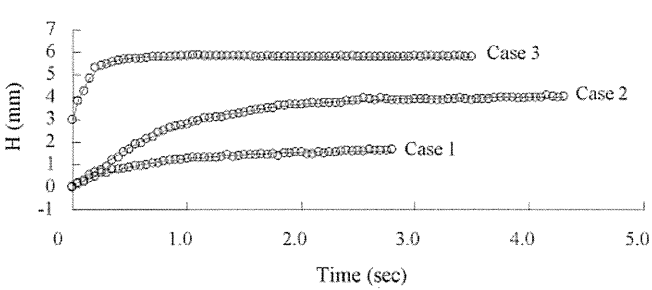

FIGURE 4. Rheological analysis of lipid layer spread in three representative cases. Each plot indicates averaged height in mm (H) of cropped spreading lipid layer, and individual exponential lines indicate the fitted curve on the basis of the Voigt model for the cases. The adapted formula was $H(t) = 0.08 - 1.54 \times \exp(-t/0.68)$ (mm) and $H'(0) = 2.25$ (mm/s) in case 1, $H(t) = 0.02 - 4.00 \times \exp(-t/0.79)$ (mm) and $H'(0) = 5.04$ (mm/s) in case 2, and $H(t) = 2.96 - 2.85 \times \exp(-t/0.14)$ (mm/s) and $H'(0) = 20.52$ (mm/s) in case 3.

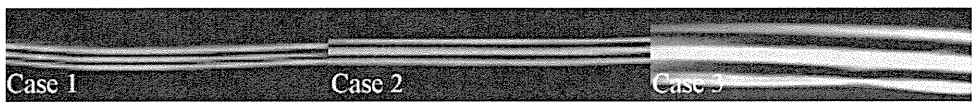

FIGURE 5. Video-meniscometer-detected images from the central lower tear meniscus in three representative cases. R = 0.09 (mm) in case 1, R = 0.14 (mm) in case 2, and R = 0.45 (mm) in case 3.

spring and the viscous flow by a dashpot (i.e., a viscous damping system; Fig. 7). If a stress σ_1 is suddenly applied at time t = 0 and held constant thereafter, the linear differential equation can be solved to give

$$\gamma = (\sigma_1/\kappa)[1 - \exp(-t/\tau)] \quad (2)$$

where $\tau = \eta/\kappa$. That is, the shear does not rise instantaneously to a fixed value (as would occur with a purely elastic body) but rises asymptotically to this value. We can suppose that, in the case of the TFLL, the applied stress σ_1 is related to the surface tension forces pulling the lipid layer upward and that the resultant shear (or observed linear displacement) of the lipid front $H(t)$ corresponds to the shear parameter γ in the Voigt model. Hence, the resemblance between the exponential terms of the two expressions suggests a possible viscoelastic property of the tear film that will influence its spread. In relation to the above, Berger and Corrsin[12] analyzed the movement of particles in the tear film after a blink, taking them to be components of the TFLL. On this basis they concluded that immediately after the blink, the TFLL was displaced, like a spring being stretched, and that the spring (the TFLL) was then allowed to return to its equilibrium position. This approach gives rise to an exponential equation similar to the Voigt model but may better reflect what happens. In addition, it seems that there is no lipid layer above the boundary seen in Figure 1, but inspection of Figure 1 indicates that a thin lipid layer is in fact present. To explain this, it has been proposed that TFLL spread consists of two events: first, that in the upstroke of the blink, a polar (largely phospholipid) layer spreads over the aqueous subphase; and second, that the nonpolar lipids (chiefly cholesterol and sterol esters, the greater part of the meibomian secretion) spread over the phospholipid layer.[30,31] Therefore, it is reasonable to conclude that a finite surface tension gradient causes the upward velocity of the TFLL rather than a discontinuity of surface tension at the border, which would theoretically cause infinite velocity at that point.

Owens and Phillips[12] also reported that the spreading velocity of particles on the tear film is adequately described by a logarithmic function. Because the particles they observed appeared to be located in the lipid film, their report may be taken to reflect the velocity of the spreading TFLL.

Curve fitting to the data, shown in Figure 4, indicates that for each of the cases studied, the relationship is of the form $H(t) - H(0) = \rho[1 - \exp(-t/\lambda)]$. Differentiation of this with respect to time gives $H'(t) = \rho/\lambda \times \exp(-t/\lambda)$. The velocity of particles observed by Owens and Phillips[12] can also be described in exponential form as (velocity) = $k_1 \times \exp(-k_2 t)$, where k_1 and k_2 are constants. It can then readily be seen that this leads to a positional formula (position) = const.$[1 - \exp(-k_2 t)]$ similar to ours and that the particle motion follows the same form as our TFLL spread. This strengthens the suggestion of Owens and Phillips[12] that the particles are embedded in and move with the lipid layer, though the sizes of these particles suggest that they may also project into the aqueous layer. Although this might help to explain our observed connection between TFLL spreading rate and tear volume, we did not notice such particles in the image samples of the TFLL images we studied.

Statistical analysis of the relationship between R and the other parameters, including $H(0)$, ρ, and λ, showed a strong and statistically significant relationship between R and ρ. However, there was no statistically significant correlation between R and λ, yet there was a weak, though statistically insignificant, correlation in the relationship between R and $H(0)$. It can theoretically be expected that the time constant, λ, correlates with the meniscus radius, R, and that one might expect equilibrium to occur more quickly when the tear film is thicker (greater meniscus radius), yet no correlation was found in the cases we studied. However, the correlation with statistical significance similar to that between R and $H'(0)$ was found between R and ρ. This is reasonable, taking the Voigt model (equation 2) into consideration, because λ in our empiric equation corresponds to τ (i.e., η/κ of equation 2, where both η and κ are material, intrinsic properties of the TFLL and are unrelated to R). Moreover, considering $H'(0) = \rho/\lambda$ and the significant correlation between $H'(0)$ and R obtained from our result, a significant correlation between R and ρ is also reasonably expected, where ρ is concerned with the equilibrium value for lipid spread and implies how high the lipid layer can spread along the y-direction; a lower height for lipid layer spread can be expected when the tear film is thinner (lower meniscus radius) because a thicker aqueous layer would be expected to allow the lipid layer to be carried higher.

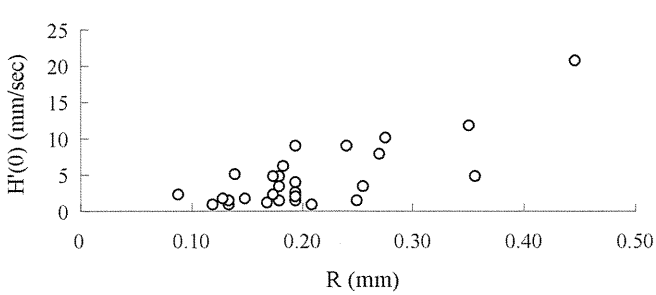

FIGURE 6. Relationship between the radius of the central lower tear meniscus (R) and the initial upward velocity of spreading TFLL, $H'(0)$, where $H'(0) = dH(0)/dt$. There was a statistically significant correlation between R and $H'(0)$ (r = 0.573; P = 0.003).

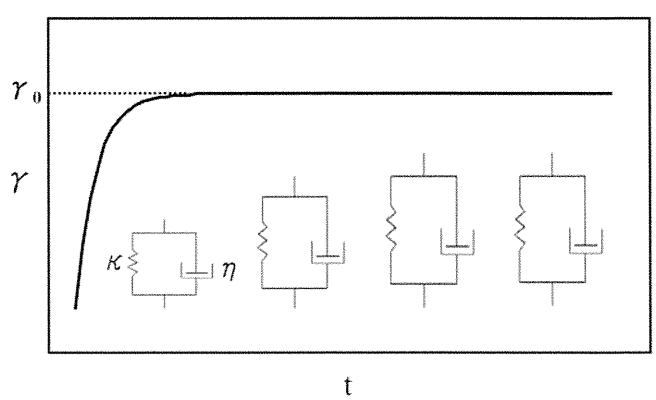

FIGURE 7. The Voigt model in rheology ($\gamma = \gamma_0[1 - \exp(-t/\lambda)]$, where γ = extent of stretch, γ_0 = γ at $t = \infty$, t = time (s), λ = retardation time (s) = η/κ, η = viscosity, κ = elasticity), consisting of a spring (κ = elasticity) and a dashpot (η = viscosity) in juxtaposition.

The findings of this study show that the Voigt model, a simple mechanistic rheological model, could successfully be adopted for analysis of the time-dependent TFLL spread in all cases studied. This suggests that the tear film is a viscoelastic material, in accordance with data showing that meibomian oil has shear-dependent viscosity and demonstrates shear thinning, which is characteristic of some viscoelastic fluids (Tiffany JM, unpublished observations, 2000).

A study by Goto and Tseng[11] of the speed of lipid layer spreading indicated that the time required for the lipid layer to stabilize after a blink was longer than normal in aqueous tear-deficient dry eyes but was shortened after punctal occlusion. This implied a normalization of the speed of spreading by the restoration of tear volume. However, the diagnosis of dry eye in that study was made by a Schirmer-based fluorescein clearance test, and tear volume was not estimated.

In a previous study we were able to show that the meniscus radius is directly related to the total tear volume over the ocular surface.[23] Furthermore, the formula given by Creech et al.[32] suggests that the precorneal aqueous layer thickness is proportional to the meniscus radius. Our present study has shown a positive relationship between meniscus radius and initial velocity of the TFLL spread, which strongly supports the concept that this parameter is influenced by tear volume, particularly tear film thickness. Thus, it is likely that the slowed initial velocity of the TFLL spread in our patients with aqueous-deficient dry eye was related to reduced tear film thickness.

The relationship between the tear film thickness and the initial velocity of the TFLL can be explained based on the model by Berger and Corrsin.[12] Their analysis could be roughly described as a viscoelastic model in which the elastic component is provided by the TFLL, whereas the viscous component is attributed to the whole thickness of the tears, particularly the aqueous layer. They assume that surface tension is inversely related to the concentration of a surfactant (presumably related to lipid layer thickness); when the tear surface is stretched, the surfactant concentration is reduced and the surface tension increases. Thus, the lipid layer behaves like an elastic membrane whose tension increases when it is stretched. Moreover, according to their model, the force-per-unit area on the lipid layer is $dT/dx = \mu \cdot v/h$, where T is the surface tension, x is the vertical position on the cornea, μ is the viscosity of the (aqueous) tear film, v is the upward velocity of the lipid layer, and h is the thickness of the (aqueous) tears. Rearranged, $v = (h/\mu) \cdot dT/dx$, and upward velocity is thus proportional to tear film thickness.

If a low tear meniscus volume implies a low tear film thickness and a low tear film thickness is responsible for slow spreading of the TFLL, either the meniscus radius or the TFLL spreading rate could be used as an index of low aqueous volume and, therefore, of aqueous-deficient dry eye. In addition, because a low tear volume is considered to contribute to dry eye symptoms through a mechanism involving shear stress, which may increase friction during blinking,[33,34] it will be of interest to study the relationship between TFLL spread and dry eye symptoms.

Although our method of analysis provides a useful quantitative approach, some limitations must be overcome in the future. Thus, we can only measure the area of the spreading TFLL if the uppermost border of the layer is well defined; cases with poorly defined borders were excluded from the present study. It has been noted that the interference image profile changes from a series of horizontal wave fronts in healthy subjects to a vertical disposition in patients with meibomian gland disease (MGD).[10] Therefore, it could prove difficult to diagnose aqueous-deficient dry eye by such a method in the presence of MGD. In addition, analysis of the spreading using graphic software was time consuming. New image-processing computer algorithms and analytical techniques are in development and should permit analysis of all interference patterns automatically in the near future.

In conclusion, our study has demonstrated that the time-dependent changes of the TFLL spread are consistent with a simple Voigt rheological model, implying viscoelastic properties of the tear film. Moreover, the initial velocity of the TFLL spread after a blink increases steadily with increase of the radius of the tear meniscus, suggesting that the rheological behavior of the TFLL is influenced by aqueous tear film thickness over the cornea. Therefore, it may be expected that the initial velocity of movement of the spreading TFLL could provide a noninvasive and quantitative parameter for the screening of aqueous tear-deficient dry eye, and the rheological analysis of the TFLL spread could potentially open a new field of research of the TFLL.

References

1. Mishima S, Maurice DM. The oily layer of the tear film and evaporation from the corneal surface. *Exp Eye Res.* 1961;1:39-45.
2. McDonald JE. Surface phenomena of the tear film. *Am J Ophthalmol.* 1969;67:56-64.
3. Norn MS. Semiquantitative interference study of fatty layer of precorneal film. *Acta Ophthalmol (Copenh).* 1979;57:766-774.
4. Doane MG. An instrument for in vivo tear film interferometry. *Optom Vis Sci.* 1989;66:383-388.
5. Yokoi N, Takehisa Y, Kinoshita S. Correlation of tear lipid layer interference patterns with the diagnosis and severity of dry eye. *Am J Ophthalmol.* 1996;122:818-824.
6. Brown SI, Dervichian DG. Hydrodynamics of blinking: in vitro study of the interaction of the superficial oily layer and the tears. *Arch Ophthalmol.* 1969;82:541-547.
7. Holly FJ, Lemp MA. Tear physiology and dry eyes. *Surv Ophthalmol.* 1977;22:69-87.
8. Wong H, Fatt II, Radke CJ. Deposition and thinning of the human tear film. *J Colloid Interface Sci.* 1996;184:44-51.
9. Bron AJ, Tiffany JM, Gouveia SM, Yokoi N, Voon LW. Functional aspects of the tear film lipid layer. *Exp Eye Res.* 2004;78:347-360.
10. Goto E, Tseng SC. Differentiation of lipid tear deficiency dry eye by kinetic analysis of tear interference images. *Arch Ophthalmol.* 2003;121:173-180.
11. Goto E, Tseng SC. Kinetic analysis of tear interference images in aqueous tear deficiency dry eye before and after punctal occlusion. *Invest Ophthalmol Vis Sci.* 2003;44:1897-1905.
12. Berger RE, Corrsin S. A surface tension gradient mechanism for driving the pre-corneal tear film after a blink. *J Biomech.* 1974;7:225-238.
13. Owens H, Phillips J. Spreading of the tears after a blink: velocity and stabilization time in healthy eyes. *Cornea.* 2001;20:484-487.
14. Bron AJ, Abelson MB, Ousler G, et al. Methodologies to diagnose and monitor dry eye disease: report of the Diagnostic Methodology Subcommittee of the International Dry Eye Workshop (2007). *Ocul Surf.* 2007;5:108-152.
15. Schirmer O. Studien zur Physiologie und Pathologie der Tränenabsonderung und Tränenabfuhr. *Albrecht von Graefes Arch Klin Exp Ophthalmol.* 1903;56:197-291.
16. Lemp MA, Hamill JR Jr. Factors affecting tear film breakup in normal eyes. *Arch Ophthalmol.* 1973;89:103-105.
17. Miyata K, Amano S, Sawa M, Nishida T. A novel grading method for superficial punctate keratopathy magnitude and its correlation with corneal epithelial permeability. *Arch Ophthalmol.* 2003;121:1537-1539.
18. van Bijsterveld OP. Diagnostic tests in the sicca syndrome. *Arch Ophthalmol.* 1969;82:10-14.
19. Fox RI, Robinson CA, Curd JG, Kozin F, Howell FV. Sjögren's syndrome: proposed criteria for classification. *Arthritis Rheum.* 1986;29:577-585.
20. Yokoi N, Bron A, Tiffany J, Brown N, Hsuan J, Fowler C. Reflective meniscometry: a non-invasive method to measure tear meniscus curvature. *Br J Ophthalmol.* 1999;83:92-97.
21. Yokoi N, Bron AJ, Tiffany JM, Kinoshita S. Reflective meniscometry: a new field of dry eye assessment. *Cornea.* 2000;19(suppl):S37-S43.

22. Oguz H, Yokoi N, Kinoshita S. The height and radius of the tear meniscus and methods for examining these parameters. *Cornea.* 2000;19:497–500.
23. Yokoi N, Bron AJ, Tiffany JM, Maruyama K, Komuro A, Kinoshita S. Relationship between tear volume and tear meniscus curvature. *Arch Ophthalmol.* 2004;122:1265–1269.
24. Maruyama K, Yokoi N, Takamata A, Kinoshita S. Effect of environmental conditions on tear dynamics in soft contact lens wearers. *Invest Ophthalmol Vis Sci.* 2004;45:2563–2568.
25. Yokoi N, Komuro A. Non-invasive methods of assessing the tear film. *Exp Eye Res.* 2004;78:399–407.
26. Palakuru JR, Wang J, Aquavella JV. Effect of blinking on tear dynamics. *Invest Ophthalmol Vis Sci.* 2007;48:3032–3037.
27. Johnson ME, Murphy PJ. Temporal changes in the tear menisci following a blink. *Exp Eye Res.* 2006;83:517–525.
28. Holly FJ. Physical chemistry of the normal and disordered tear film. *Trans Ophthalmol Soc U K.* 1985;104(pt 4):374–380.
29. Barnes HA. *A Handbook of Elementary Rheology.* Aberystwyth, Wales: Institute of Non-Newtonian Fluid Mechanics, University of Wales; 2000:81–106.
30. Holly FJ. Tear film physiology. *Int Ophthalmol Clin.* 1987;27:2–6.
31. McCulley JP, Shine WE. The lipid layer of tears: dependent on meibomian gland function. *Exp Eye Res.* 2004;78:361–365.
32. Creech JL, Do LT, Fatt I, Radke CJ. In vivo tear-film thickness determination and implications for tear-film stability. *Curr Eye Res.* 1998;17:1058–1066.
33. Cher I. Blink-related microtrauma: when the ocular surface harms itself. *Clin Exp Ophthalmol.* 2003;31:183–190.
34. Korb DR, Herman JP, Greiner JV, et al. Lid wiper epitheliopathy and dry eye symptoms. *Eye Contact Lens.* 2005;31:2–8.

IOVS Papers in Press. Published on December 30, 2008 as Manuscript iovs.08-3046

Tight Junction Transmembrane Protein Claudin Subtypes Expression and Distribution in Human Corneal and Conjunctival Epithelium

Yusuke Yoshida,[1,2] Yuriko Ban,[1,2] and Shigeru Kinoshita[2]

From the [1] Department of Ophthalmology, Nantan General Hospital, Nantan, Japan and the [2]Department of Ophthalmology, Kyoto Prefectural University of Medicine, Kyoto, Japan

Correspondence to: Yuriko Ban, Department of Ophthalmology, Nantan General Hospital, 25 Yagiueno, Nantan, 629-0197 Japan

Phone: +81-771-42-2510. Fax: +81-771-42-2096

E-mail: yban@koto.kpu-m.ac.jp

Manuscript word count: 3,157

Financial Support: Grants-in -Aid for scientific research from the Japanese Ministry of Education, Culture, Sports, Science and Technology

Keywords: tight junction; claudin subtypes; conjunctival epithelium; corneal epithelium; occludin; immunohistochemistry

Abstract

PURPOSE: The combination of the tight-junction transmembrane protein claudin subtypes is one of the most important determinants of variations in the tightness of individual paired tight junction strands. The barrier function of corneal epithelium is much stronger than that of conjunctival epithelium. In this study, the expression and cellular distribution of claudin species in *in vivo* human corneal and conjunctival epithelium were investigated.

METHODS: Reverse transcription-polymerase chain reaction was used to reveal the claudin mRNA. Immunohistochemistry was used to determine the tissue distribution of tight junction-related proteins and MUC5AC.

RESULTS: The transcripts for claudin-1, -2, -3, -4, -7, -9, and -14 were identified in human corneal epithelium. The transcripts for claudin-1, -2, -4, -7, -9, -10, and -14 were identified in human conjunctival epithelium. By immunohistochemistry, claudin-1, -4, and -7 were found to be localized at the membrane of human corneal and conjunctival epithelial cells. In human conjunctival epithelium, claudin-10 staining was observed at several, but not all, apical epithelial cell-to-goblet cell junctions.

CONCLUSIONS: Claudin-1, -4, and -7 are expressed in both corneal and conjunctival epithelia. Claudin-10 is prominent at several junctions between apical epithelial cells and goblet cells in conjunctival epithelium. Except for the claudin-10 expression in conjunctival epithelium, the claudin subtype expression of corneal and conjunctival epithelium is similar. Therefore, there must be a difference between these two epithelium types in regards to the specific ratio of claudin subtypes that are expressed or their phosphorylation status, and that the distribution of goblet cells in conjunctival epithelium also influences the difference in barrier function.

INTRODUCTION

Corneal and conjunctival epithelium, which construct the ocular surface, form a barrier that isolates the eye from the outside environment and regulate the passive movement of fluid, electrolytes, macromolecules, and cells through the paracellular pathway. Tight junctions in the epithelium create this barrier, and together, the cornea and conjunctiva work to form this important defense for the eye. However, it is well known that the tightness of the corneal epithelium tight junction is much greater than that of conjunctival epithelium.[1, 2] Corneal epithelium is constructed by epithelial cells and has 5 or 6 layers of stratification. Conjunctival epithelium is also stratified squamous epithelium, but unlike corneal epithelium, it contains goblet cells. Goblet cells are located in the apical surface of the conjunctiva and interspersed among its multiple layers of stratified epithelium.

Tight junctions are present at the apical side of epithelia and play an important role in the establishment and maintenance of the barrier function and cell polarity. The tight junction is composed of three groups of proteins; transmembrane proteins (occludin, claudin, and junctional adhesion molecules), peripheral membrane proteins (ZO-1, Z-2, ZO-3, and MUPP-1) which have PDZ domains and bind to transmembrane proteins, and cytoplasmic proteins (cingulin, 7H6 antigen, etc.) that exist around tight junctions without any direct binding.[3]

Claudin (23kDa) is comprised of a family of transmembrane proteins that form the strands of the tight junction; 24 claudins have been identified thus far. Claudins are the only junctional proteins known to have tissue specificity. Both occludin and claudins contain four transmembrane domains, with both N and C termini oriented into the cytoplasm, but these two

proteins show no sequence similarity.[4,5,6] Different mixtures of claudins and occludin create tight-junction strands that are associated laterally with strands of adjacent cells, forming paired strands that eliminate extracellular space.[7]

We previously reported the distribution of ZO-1, occludin, and claudin in *in vivo* human corneal epithelium.[8] Immunohistochemistry has shown that in human corneal epithelium, most apical cells exhibit ZO-1, occludin, and claudin-1. By the reverse transcription-polymerase chain reaction (RT-PCR) method, the transcripts for claudin-1 and several other claudin isotypes, such as claudin-2, -3, -4, -7, -9 and -14, were identified from *in vivo* human corneal epithelium.

In this report, we examine the distribution of tight-junction proteins ZO-1, occludin, and claudins from *in vivo* human conjunctival epithelium, and try to identify the difference in the tight junction property of corneal and conjunctival epithelium.

MATERIALS AND METHODS

Tissue Preparation of the Human Corneas and Conjunctivas

The experiments conducted in this study used human corneal tissue supplied from the Northwest Lion Eye Bank (Seattle, WA) or that extirpated from patients with corneal stromal opacity diseases during penetrative keratoplasty surgery, therefore the corneal epithelium was intact. Human conjunctival tissue was obtained at the time of cataract or conjunctival chalasis surgery with proper informed consent of the patients. All experiments were done immediately after obtaining the tissue. The present study had the approval of the Nantan General Hospital ethics

committee and the procedures followed the Tenets of the Declaration of Helsinki.

Primary Antibodies

The rabbit anti-ZO-1 polyclonal antibody, rabbit anti-claudin-1 polyclonal antibody, rabbit anti-claudin-2 polyclonal antibody, rabbit anti-claudin-7 polyclonal antibody, rabbit anti-claudin-14 polyclonal antibody, and mouse anti-claudin-15 monoclonal antibody were purchased from Zymed Laboratories (South San Francisco, CA). The goat anti-occludin polyclonal antibody, goat anti-claudin-3 polyclonal antibody, goat anti-claudin-4 polyclonal antibody, goat anti-claudin-9 polyclonal antibody, and rabbit anti-claudin-10 polyclonal antibody were purchased from Santa Cruz Biotechnology (Santa Cruz, CA). The mouse anti-Muc5AC monoclonal antibody was purchased from Abcam (Cambridge, United Kingdom). Alexa 488-labeled goat anti-rabbit antibody, Alexa 488-labeled rabbit anti-goat antibody, and Alexa 594-labeled goat anti-mouse antibody were purchased from Invitrogen Corporation (Carlsbad, CA).

Immunohistochemistry

Tight-junction associated proteins were studied via indirect immunohistochemistry. For the transverse images, 7-μm cryostat sections were placed on gelatin-coated slides, air dried, and then rehydrated in phosphate buffered saline (PBS) containing 1.0 mM $MgCl^2$ and 0.1 mM $CaCl^2$ at room temperature for 15 minutes. The sections were fixed with 95% ethanol at 4°C for 30 minutes, followed by 100% acetone at room temperature for 1 minute. After several washes with PBS, sections were incubated with 1% bovine serum albumin at room temperature for 30

minutes to block nonspecific binding. Following this, the sections were incubated at 4°C for 12 hours with primary antibody, and then washed three times in PBS for 15 minutes. For negative controls, the equivalent serum was used. After staining with the primary antibodies, the sections were incubated at room temperature for 1 hour with suitable secondary antibodies and washed several times with PBS.

For the en face images, whole corneas were fixed with 95% ethanol at 4°C for 30 minutes, followed by 100% acetone at room temperature for 1 minute. After several washes with PBS, tissues were permeabilized by incubation in PBS containing 0.1%Triton X-100 for 10 minutes. Tissues were developed to the first and second antibody steps, described above. During all steps, the epithelial side was kept facing upward to avoid damage. The tissues were coverslipped using anti-fading mounting containing diamidino-2-phenylindole for nuclei staining (Vector Laboratories, Burlingame, CA). The slides were examined and we took pictures every 0.5μm slice and merged several pictures by confocal microscope (TCS SP2 AOBS; Leica Microsystems GmbH, Wetzlar, Germany).

RNA Isolation and RT-PCR Amplification of Claudin Species

For RT-PCR, human corneal epithelial sheets peeled from donor corneal buttons and excised conjunctiva, were directly lysed with reagent (Trizol; GIBCO BRL, Rockville, MD); total cellular RNA was isolated according to the manufacturer's instructions. RT-PCR was performed in accordance with the previous report by Yi et al.[9] In brief, complementary DNA was generated in the presence of 0.5 μg oligo (dT) from 5 mg total RNA with reverse transcriptase (SuperScript II; Life Technologies, Rockville, MD). We used PCR primers that Yi et al. designed for human

claudins-1 through -4, -7, -9, -10, -14, and -15. PCR products were examined by 2% agarose gel and ethidium bromide staining. The observed PCR products corresponded to their expected molecular weights.

RESULTS

Distribution of ZO-1 and Occludin in Human Conjunctival Epithelium

In the transverse sections, occludin and ZO-1 were localized at the apical superficial epithelial cell tight junctions, as well as the epithelial-cell to goblet-cell tight junctions (Fig. 1A, C). In the en face sections, occludin and ZO-1 antibodies showed as bands that corresponded to the junctional complex (Fig. 1B, D). This occludin staining was different from that of the cornea, as it is not continuous and is presented in a dot-like pattern along the cell junctions.[8]

Claudin Subtype Expression in Human Conjunctival Epithelial Cells Detected by RT-PCR

We previously reported that the transcripts for claudin-1 and several other claudin isotypes, such as claudin-2, -3, -4, -7, -9, and -14, were identified from human corneal epithelium.[8] In this study, we determined the presence of transcripts of claudin subtypes in human conjunctival epithelial cells by the same RT-PCR method. The transcripts for claudin-1, -2, -4, -7, -9, -10, and -14 were identified from conjunctival epithelium (Fig. 2). Claudin-3 was not identified in human conjunctival epithelium which existed in human corneal epithelium. On the other hand, claudin-10 was identified in conjunctival epithelium but not in corneal epithelium. No amplified claudin

mRNA was observed without reverse transcriptase (RT) (data not shown).

Distribution of Claudins in Human Conjunctival and Corneal Epithelium

Not all claudin subtypes of which transcripts were identified were expressed in conjunctival and corneal epithelium. The corneal epithelial cells through all cell layers were stained by claudin-1, -4, and -7. No staining was observed by claudin-2, -3, -9, -10, -14, and -15 (Fig. 3). In the en face images, claudin-1, -4, and -7 antibodies showed as bands that corresponded to the junctional complex (Fig. 4). In the conjunctival epithelium, claudin-1 and -4 staining was observed in all cell layers. Claudin-7 staining was observed in superficial cells (Fig. 5). In the en face images, those three claudin subtype antibodies showed as bands that corresponded to the junctional complex (Fig. 6). In addition, it was worth mentioning that some openings of goblet cells which were identified by positive reactivity with anti-MUC5 antibody showed claudin-10 staining (Fig. 5 and 6). No staining was observed by claudin-2, -3, -9, -14, and -15 (Fig. 6).

DISCUSSION

The ocular surface consists of corneal and conjunctival epithelia, both of which are stratified non-keratinized epithelium. The corneal epithelium is a transparent and flat stratified squamous epithelium devoid of goblet cells with a cuboid basal layer lying on the avascular corneal stroma by the Bowman's layer. The conjunctival epithelium is populated by goblet cells. Sequencing of mucin genes has led to the identification of two categories of mucins: secreted, and membrane associated. The conjunctival goblet cells express one of the secreted gel-forming mucins,